53rd IEEE Conference on Decision and Control
December 15-17, 2014. Los Angeles, California, USA

Viability and analysis of implementing only voltage-power droop for parallel inverter systems

Srinivasa Salapaka, Brian Johnson, Blake Lundstrom, Sangsun Kim, Scott Collyer, and Murti Salapaka.

Abstract— **In microgrids that are predominantly resistive, real and reactive power can be controlled by implementation of voltage and frequency droop laws respectively. However, the variable frequency displayed by such a system complicates analysis such that design approaches rely on approximations and linearized models. In this work, we present a modified form of droop control where only the voltage versus real power relationship is upheld and the frequency is held constant. Since the frequency is not explicitly controlled and the reactive power is not measured, the controller can be simplified. In such a setting, the only assumption we make is that all inverters have access to a common time-reference. Because fixed frequency operation is enforced by design, a variety of analytical tools can be leveraged to formulate a comprehensive analytical framework which facilitates a precise design methodology. In particular, closed-form expressions on the output current phase differences are obtained which yield practical selection guidelines on the voltage-power droop gains such that reactive flows between inverters are kept small. As a corollary, it is demonstrated that there are no reactive power flows in the presence of purely resistive loads. For the particular case of a single inverter, an almost exact solution describing the nonlinear dynamics of the inverter output voltage, current, and power are derived. Accompanying simulation results validate the analytical results and demonstrate the feasibility of the proposed control approach.**

I. Introduction

Microgrids are small-scale power systems which utilize local power generation and are generally expected to operate in both grid-connected and islanded modes such that uninterruptible power is delivered to local loads [1], [2], [3]. Because generation is placed in close proximity to loads, a bottom-up approach to system design can be emphasized. Of particular importance is the utilization of modular renewable energy sources, such as wind and photovoltaics, and their accompanying power electronic inverter interfaces. Droop control is a technique which has been applied widely in inverter-based system such that system voltage and frequency stability is maintained while ensuring synchronization [4].

In essence, droop control is a technique of controlling inverters such that they approximate the dynamics of coupled synchronous machines in power systems. However, the variable frequency exhibited by droop controlled systems complicates analysis which often is overcome through linearized models and assumptions on system impedances [5], [6]. In [7], [8], power-flow based phenomenological dynamic models that incorporate droop laws for frequency synchronization and voltage control are analyzed. Sufficient conditions for voltage stability in terms of inequality constraints on various network parameters, the loads, and generation set points are derived in [7]. A quadratic droop law is introduced in [8] which enables analysis of the equilibrium points under the corresponding model such that closed-form load conditions for voltage stability are attained. An improved droop law that achieves more accurate proportional load sharing and is robust to component mismatches, parameter drifts, and disturbances is proposed in [9].

In this work, we focus our investigation on inverter-based microgrids with predominantly resistive networks and propose a simplified droop controller which acts only on the real power output of each inverter. By assuming the existence of a common time-reference among inverters (that is, *isochronous* operation), the system is designed to operate at a single frequency despite system disturbances. For networks with small X/R ratios, it is conventional to modulate the inverter voltage and frequency inversely with respect to the real and reactive power output, respectively [10]. However, in contrast to established techniques, we adopt a simplified and isochronous incarnation of droop control where each voltage set-point is altered with respect the real power output and the system frequency is fixed. In such a setting, it is not necessary to measure and compute the reactive power and isochronous operation is facilitated by a common time reference between inverters. We also supplement the controller with a virtual resistance such that network inductances are subsumed. Since isochronous operation is enforced by design, the development of a comprehensive analytical and design framework which describes both steady-state and dynamic parameters is facilitated.

In our analysis, we focus on control architectures that contain a slow droop-based outer loop which derives a sinusoidal voltage reference and a fast inner loop which consists of both a current and voltage controller. This is in contrast to previous analytical efforts which exclude

S. Salapaka is with Mechanical Science and Engineering at the University of Illinois, Urbana, IL 61801, email: salapakas@google.com

B. Johnson and B. Lundstrom are with the National Renewable Energy Laboratory (NREL), Golden, Colorado, USA. NREL is a national laboratory of the U.S. Department of Energy, Office of Energy Efficiency and Renewable Energy, operated by the Alliance for Sustainable Energy, LLC, email: {brian.johnson,blake.lundstrom}@nrel.gov

S. Kim and S. Collyer are with Google Inc, email: {sskim,scollyer}@google.com

M. Salapaka is with Electrical and Computer Engineering at the University of Minnesota,Twin Cities, MN 55455, email: salapakam@google.com

The authors acknowledge A. Mazumdar, A. Ramesh, J. Sastry, D. Fork, and R. Koningstein for their insightful discussions, help, and support of this work.

fast inner-loop controllers from analysis and are focused exclusively on the slow droop dynamics. Furthermore, we assume that the design of the inner controller is based on the internal model principle such that the steady-state error at the nominal frequency is zero. Under such conditions, closed-form relationships of the output current phase differences are derived. Despite the fact that the inverter voltage angles and reactive power are not explicitly controlled, we show that the reactive power flows between inverters can be kept small by proper selection of the droop gains and we prove that reactive power flows are zero in the case of a purely resistive load. Bounds on the system voltage in terms of the active power commands and uncertainty in loads are also obtained and the impact of the virtual resistance on system performance is analyzed. Lastly, an almost exact solution describing the nonlinear dynamics of the output voltage, current, and power of a single inverter is derived. Simulation results confirm the validity of the analytical framework and demonstrate the feasibility of the proposed control approach.

II. System description

Consider the network of N inverters connected in parallel across a common load, as shown in Fig. 2 To facilitate analysis, high-frequency switching dynamics are disregarded and we model the averaged dynamics [11] of the k^{th} inverter as a controllable voltage source as shown in Fig. 1. By using

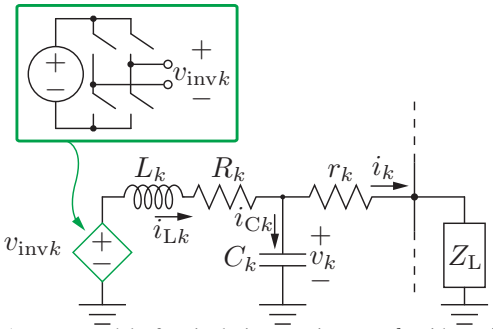

Fig. 1. Average model of a single inverter instance k with an LC filter and a linear load $Z_L(s)$. The parasitic resistance of the inductor windings are encapsulated in R_k and the line resistance is denoted by r_k.

Kirchoff's laws for the circuit in Fig. 1, we obtain

$$\hat{v}_k = \underbrace{\frac{\hat{v}_{\text{inv}k}}{L_kC_ks^2 + R_kC_ks + 1}}_{G_{vinv,k}} - \underbrace{\frac{(L_ks + R_k)\hat{i}_k}{L_kC_ks^2 + R_kC_ks + 1}}_{G_{\text{i}k}}, \tag{1}$$

where $\hat{x}(s)$ represents the Laplace transform of $x(t)$, $v_{\text{inv}k}$ is the control signal of the k^{th} inverter, and the output voltage v_k, inductor current $i_{\text{L}k}$, and output inverter current i_k are measured signals. Therefore for the control law of the form $\hat{v}_{\text{inv}k} = K_{\text{ref}k}\hat{v}_{\text{ref}k} - K_{\text{v}k}\hat{v} + K_{\text{i}k}\hat{i}_k$, the closed-loop system for the k^{th} inverter is given by

$$\begin{aligned}\hat{v}_k \;=\; & (1 + G_{\text{inv}k}K_{\text{v}k})^{-1}G_{\text{inv}k}K_{\text{ref}k}\hat{v}_{\text{ref}k} + \\ & (1 + G_{\text{inv}k}K_{\text{v}k})^{-1}(G_{\text{inv}k}K_{\text{i}k} - G_{\text{i}k})\hat{i}_k,\end{aligned} \tag{2}$$

where $v_{\text{ref}k}$ is the sinusoidal reference voltage generated by the droop controller (see Fig. 2). Therefore the dynamics of N inverters are described by $\hat{\boldsymbol{v}} = T\hat{\boldsymbol{v}}_{\text{ref}} + Q\hat{\boldsymbol{i}}$, where $\hat{\boldsymbol{v}} := \begin{bmatrix}\hat{v}_1 & \cdots & \hat{v}_N\end{bmatrix}^T$, $\hat{\boldsymbol{v}}_{\mathbf{ref}} := \begin{bmatrix}\hat{v}_{\text{ref}1} & \cdots & \hat{v}_{\text{ref}N}\end{bmatrix}^T$, $\hat{\boldsymbol{i}} := \begin{bmatrix}\hat{i}_1 & \cdots & \hat{i}_N\end{bmatrix}$, $T := \text{diag}(T_1, \ldots, T_N)$, $Q := \text{diag}(Q_1, \ldots, Q_N)$, $T_k := (1 + G_{\text{inv}k}K_{\text{v}k})^{-1}G_{\text{inv}k}K_{\text{ref}k}$, and $Q_k := (1 + G_{\text{inv}k}K_{\text{v}k})^{-1}(G_{\text{inv}k}K_{\text{i}k} - G_{\text{i}k})$. Further, if we assume that the load is linear given by $\hat{\boldsymbol{i}} = Y(s)\hat{\boldsymbol{v}}$, where $Y(s)$ is the admittance matrix of the network (see Fig. 2), then the closed-loop expressions for $\hat{\boldsymbol{v}}$ and $\hat{\boldsymbol{i}}$ are

$$\hat{\boldsymbol{v}} = (I - QY)^{-1}T\hat{\boldsymbol{v}}_{\text{ref}}, \quad \hat{\boldsymbol{i}} = Y(I - QY)^{-1}T\hat{\boldsymbol{v}}_{\text{ref}}.$$

Also from the network in Fig. 2 with N branch resistances r_k for $k = 1, \ldots, N$, the voltage across the load Z_L is given by

$$\hat{v}_L = h(s)\sum_{k=1}^{N}\frac{\hat{v}_k}{r_k}, \tag{3}$$

where $h(s)^{-1} := r_1^{-1} + \cdots + r_N^{-1} + Z_L^{-1}$ and

$$\hat{i}_L = \frac{\hat{v}_L}{Z_L(s)} = \frac{h(s)}{Z_L(s)}\sum_{m=1}^{N}\frac{\hat{v}_m}{r_m} = q(s)\sum_{m=1}^{N}\frac{\hat{v}_m}{r_m}, \tag{4}$$

where $q(s) := h(s)/Z_L(s)$. The k^{th} inverter current, i_k, is given by

$$\hat{\boldsymbol{i}} \;=\; (\boldsymbol{\Lambda} - h\boldsymbol{\lambda}\boldsymbol{\lambda}^{\text{T}})\hat{\boldsymbol{v}} = Y\hat{\boldsymbol{v}} \tag{5}$$

where $Y := (\boldsymbol{\Lambda} - h\boldsymbol{\lambda}\boldsymbol{\lambda}^{\text{T}})$, $\boldsymbol{\lambda} = [r_1^{-1}, \ldots, r_N^{-1}]^{\text{T}}$, and $\boldsymbol{\Lambda} = \text{diag}(r_1^{-1}, \ldots, r_N^{-1})$.

A. The droop model

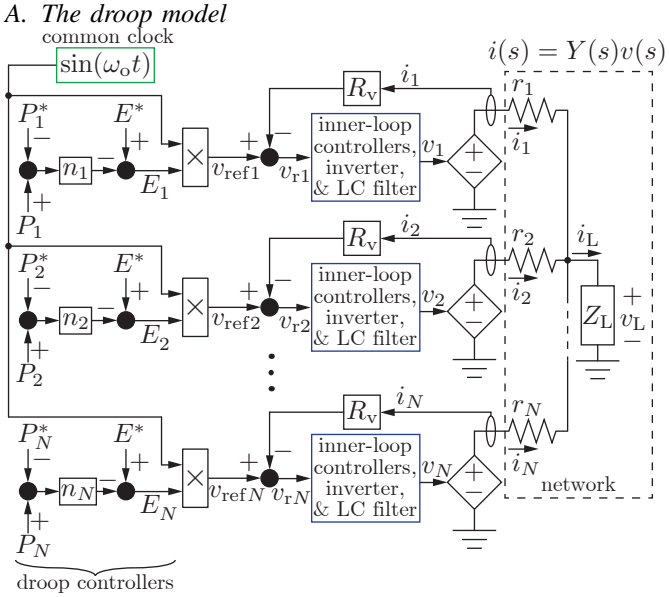

Fig. 2. A system of N parallel inverters that provide power to a load with impedance $Z_L(s)$. The details of the outer-loop droop controllers and network are shown.

The voltage–power droop law, which determines the sinusoidal reference voltage for each inverter, is given by

$$v_{\text{ref}k}(t) = [E^* - n_k(P_k - P_k^*)]\sin\omega_{\text{o}}t, \tag{6}$$

where ω_{o} is the rated system frequency and n_k is the k^{th} droop gain. Note that all inverters have access to a common time-reference, t. Rewriting (6) in matrix form yields

$$\boldsymbol{v}_{\text{ref}k}(t) = [E^*\mathbf{1} - \mathcal{N}(\boldsymbol{P} - \boldsymbol{P}^*)]\sin\omega_{\text{o}}t,$$

where $\mathcal{N} = \text{diag}(n_1, \ldots, n_N)$. The active power utilized by each droop controller is derived from the instantaneous power $p_k(t) := v_k(t)i_k(t)$ via a first order filter with time constant τ_P. Thus,

$$\hat{P}_k = \frac{1}{\tau_P s + 1} \hat{p_k}. \tag{7}$$

B. Inner-control-loop model

The inner control loop is composed of cascaded voltage and current controllers. As shown in Fig. 3, the voltage controller acts on the sinusoidal reference generated by the outer droop controller. In turn, the voltage controller outputs a sinusoidal current reference, i_{ref}, which is processed by an innermost current controller. As outlined in [11], the main advantage of this structure is increased robustness of the inverter voltage to load variations. Note that the virtual resistance, R_v, is incorporated by subtracting an iR_v voltage drop from the voltage reference.

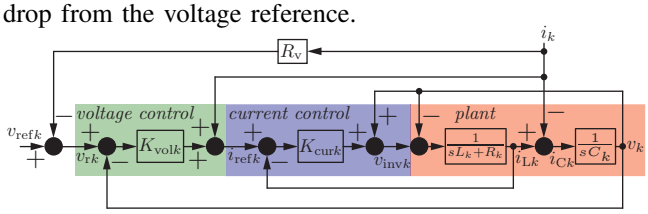

Fig. 3. The inner-control loop for voltage regulation with a virtual resistance. The transfer functions of the voltage and current compensators are given by K_{vol} and K_{cur}, respectively.

Referring to Fig. 3, it follows that

$$\hat{v}_{\text{inv}} = K_{\text{lverf}}\hat{v}_{\text{ref}} - \tilde{K}_\text{v}\hat{v} + K_\text{v}\hat{i} + K_{i_L}\hat{i}_L, \tag{8}$$

where $K_{\text{lverf}} = K_{\text{cur}}K_{\text{vol}}$, $\tilde{K}_\text{v} = K_{\text{cur}}K_{\text{vol}} - 1$, $\tilde{K}_\text{i} = K_{\text{cur}} - K_{\text{cur}}K_{\text{vol}}R_\text{v}$, $K_{i_L} = -K_{\text{cur}}$.

III. Dynamics of a Single Inverter Driving a Linear Load

In this section, an approximate solution with quantifiable error bounds for an inverter driving a linear load is obtained. Consider a single inverter driving an impedance load where the measured power, P, is given by (7). For the remaining analysis in this section, indices are dropped since we are studying a single unit. We assume that the time constants of the voltage and current dynamics in (8) are much faster than the dynamics of the active power equation (7). Thus, with respect to the voltage and the current dynamics, the power P is approximated as being constant. In other words, both v and i reach their steady-state values before any appreciable change occurs in P.

For a given P, the product $v(t)i(t)$ at steady-state is given by $\frac{1}{2}|(I - QY)^{-1}T|^2|Y(j\omega_\text{o})|E^2(P)\cos(\angle(Y(j\omega_\text{o})) - \cos(2\omega_\text{o}t + \phi_i + \phi_v)$, where $E(P) = [E^* - n(P - P^*)]$, $\phi_v = \angle((I - QY)^{-1}T|_{s=j\omega_\text{o}})$, and $\phi_i = \angle(Y(I - QY)^{-1}T|_{s=j\omega_\text{o}})$. Therefore from (7) we obtain

$$\tau_P \frac{dP}{dt} + P(t) = \alpha E^2(P)\left(1 - \frac{\cos(2\omega_\text{o}t + \phi_i + \phi_v)}{\cos(\angle(Y(j\omega_\text{o}))}\right) \tag{9}$$

where $\alpha = \frac{1}{2}|(I - QY)^{-1}T|^2|Y(j\omega_\text{o})|\cos(\angle(Y(j\omega_\text{o}))$. Note that in the above time-varying nonlinear differential equation, the time constant τ_p is designed to be large such that the low-pass filter has a small bandwidth. As a result, the filter rejects the sinusoidal term with frequency $2\omega_\text{o}$ in (9). Therefore, by design, $\epsilon := 1/(\omega_\text{o}\tau_p) \ll 1$ and is typically in the range of 10^{-3}–10^{-4}.

Theorem 1: There exist constants $L > 0$ and $c > 0$ such that the solution $P(t)$ to (9) with initial condition $P(0)$ satisfies

$$\|P(t) - \bar{P}(t)\| \leq c\epsilon \quad \text{for } 0 \leq t \leq L\tau_p, \tag{10}$$

where

$$\bar{P}(t) = \frac{a\beta^{-1}(t) - b}{\beta^{-1}(t) - 1}, \tag{11}$$

is the approximate solution of (9), $\epsilon := 1/(\omega_\text{o}\tau_p)$, $(2\alpha n^2 a, 2\alpha n^2 b) = 2n\alpha(E^* + nP^*) + 1 \pm \sqrt{4\alpha n(E^* + nP^*) + 1}$, and $\beta(t) = \frac{(P(0)-a)}{(P(0)-b)}e^{\frac{a-b}{\alpha n^2 \tau_P}t}$.

Proof: See Appendix

A. Simulation Results

In this section, the control implementation summarized in Figs. 2– 3 is evaluated with a single inverter driving a constant impedance load. The load is designed to consume 3 kW of real power at a power factor of 0.8. In addition, $n = 0.2\,\text{V/W}$, $r = 0.1\,\Omega$, $P^* = 1.5\,\text{kW}$, $E^* = 120\sqrt{2}\,\text{V}$. and $\tau_P = 0.1\,\text{s}$. The time-domain waveforms in Fig. 4(a) compare the evolution of the approximate power response in (11) and the numerical solution to (9). Along similar lines, the approximate and numerically-simulated inverter voltages using are compared in Fig. 4(b). The results confirm that the approximate solution given in Theorem 1 provides a nearly exact solution to active power and voltage signals.

IV. Multi-Inverter System Analysis

To begin, we assume that the branch resistance between each inverter LC filter and the load is purely resistive. As illustrated in Figs. 2– 3, the inner control loop has the objective of tracking the sinusoidal voltage reference given by $v_{r,k}(t) = E_k \sin\omega_\text{o}t - R_\text{v}i$.

Theorem 2: Consider the inner control loop shown in Fig. 3. Suppose $K_{\text{vol}k}$ has a factor $\frac{1}{s^2+\omega_\text{o}^2}$ and the closed-loop system is stable. Also, suppose that $v_{\text{ref}k}(t)$ and $i_k(t)$ are sinusoids with frequency ω_o. It follows that in steady-state

$$v_k(t) = v_{r,k}(t), \tag{12}$$

where $v_{r,k}(t)$ is the voltage reference processed by the k^{th} inner-loop controller and $v_{r,k}(t) = v_{\text{ref}k}(t) - R_\text{v}i_k(t)$. Thus, if all external inputs to the system in Fig. 3 (that is $v_{\text{ref}k}$ and i) are sinusoidal with frequency ω_o, then the inverter voltage follows the sinusoidal reference with zero steady-state error. Furthermore $T(j\omega_\text{o}) = 1$ and $Q(j\omega_\text{o}) = R_\text{v}$.

Proof: The proof is omitted for space reasons.

The following theorem establishes that despite the absence of explicit control over reactive power, voltage phase angle, and frequency, there will be no extraneous reactive power flows if the load is purely resistive.

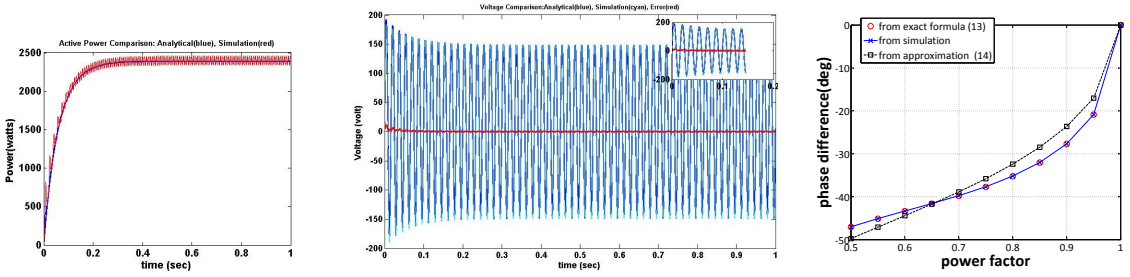

(a) (b) (c)

Fig. 4. (a) Comparison of the approximated and numerically simulated power waveforms, $P(t)$ and $\bar{P}(t)$, respectively. (b) The approximated and simulated inverter voltage waveform. (c) Phase differences in inverter currents for a system with two inverters. We consider the case where $P_2^* = 3P_1^*$, $P_1^* + P_2^* = 6$ kW, $[L, R, C] = [600\,\mu\text{H}, 0\,\Omega, 100\,\mu\text{F}]$, rated load power is 6 kW, $n_1 = n_2 = 0.05$ V/W, and examine behavior over a range of load power factors. The phase differences computed using (13) and (14) match results from the numerical simulations.

Theorem 3: Suppose the conditions of Theorem 2 hold and the load is purely resistive such that $Z_L(s) = R_L$. In steady-state, the voltage and current output of the k^{th} inverter is given by $v_k(t) = V_k \sin \omega_o t$ and $i_k(t) = I_k \sin \omega_o t$ for $V_k, I_k \in \mathbb{R}_+$.

Proof: The proof is omitted for space reasons.

Next, we characterize the phase difference between inverter currents, i_k and i_j, in the general setting with complex impedance loads.

Theorem 4: Let $\delta_k = (E_k - E^*)/E^*$, $\boldsymbol{\delta} = [\delta_1, \ldots, \delta_N]^{\mathrm{T}}$, $\boldsymbol{\lambda}_v := [(r_1 + R_{\mathrm{v}})^{-1}, \ldots, (r_N + R_{\mathrm{v}})^{-1}]^{\mathrm{T}}$, $\boldsymbol{\xi} = \frac{\boldsymbol{\lambda}_v}{\boldsymbol{\lambda}_v \mathbf{1}}$, $\nu = (Z_L \boldsymbol{\lambda}_v^{\mathrm{T}} \mathbf{1})/(1 + Z_L \boldsymbol{\lambda}_v^{\mathrm{T}} \mathbf{1})$, and suppose the conditions in Theorem 2 hold. Then $\tan(\phi_k - \phi_j)$, where ϕ_m denotes the phase of i_m, is given by

$$\frac{\mathrm{Im}(\nu)\dfrac{\delta_k - \delta_j}{1 + \boldsymbol{\xi}^{\mathrm{T}}\boldsymbol{\delta}}}{\left(\mathrm{Re}(\nu) - \dfrac{1+\delta_k}{(1+\boldsymbol{\xi}^{\mathrm{T}}\boldsymbol{\delta})}\right)\left(\mathrm{Re}(\nu) - \dfrac{1+\delta_j}{(1+\boldsymbol{\xi}^{\mathrm{T}}\boldsymbol{\delta})}\right) + \mathrm{Im}(\nu)^2}. \tag{13}$$

Proof: See Appendix.

Remark 1: Note that if the load Z_L is real, then the phase differences between inverter currents are zero. This also follows from Theorem 3.

The following corollary provides a more intuitive expression for the phase difference between currents which can provide practical guidelines for design.

Corollary 1: Assume the notation and the assumptions of Theorem 4. Suppose $\delta_k = O(\epsilon)$ and $|Z_L \boldsymbol{\lambda}^{\mathrm{T}} \mathbf{1}| \gg 1$ then

$$\tan(\phi_k - \phi_j) \approx \left(\sum_m \frac{|Z_L| \sin\theta_L}{r_m + R_{\mathrm{v}}}\right)(\delta_k - \delta_j). \tag{14}$$

Remark 2: If E_k is close to E^*, which in turn yields small $\delta_k := (E_k - E^*)/(E^*) = \sum_m 1/(r_m + R_{\mathrm{v}})$, then it is expected that $\delta_k - \delta_j$ is small. Typically, the branch resistance, r_k, and virtual resistance, R_{v}, are both small, when compared to $|Z_L|$. Consequently, $|Z_L \boldsymbol{\lambda}_{\mathrm{v}}^{\mathrm{T}} \mathbf{1}| \gg 1$ should also hold. Thus, the assumptions in Corollary 1 are not restrictive (see Fig. 4(c) for verification of analytical expressions through simulations).

Remark 3: The relationship in (14) establishes that the inverter current phase differences are small for those designs that achieve values of E_k close to E^*. In particular, for the current phase differences to be smaller than $\epsilon \ll 1$, it follows that $|\delta_k - \delta_j| \leq \epsilon \frac{\sum_m \frac{1}{r_m + R_{\mathrm{v}}}}{|Z_L| \sin\theta_L}$ needs to be satisfied.

Remark 4: The amplitude of the voltage at the inverter output, $v_k = E_k \sin \omega_o t - R_{\mathrm{v}} i_k$, depends on the inverter current i_k where the nature of this dependence is not straightforward. However, the expression in (14) depends only on E_k since $\delta_k = (E_k - E^*)/E^*$. Recalling $E_k = E^* - n_k(P_k - P_k^*)$, it is evident that the deviation of E_k from E^* is dictated by the outer droop law. Thus, the analysis above translates the concerns of limiting reactive flows exclusively to the design of the outer droop law.

A. Bounds on voltage deviations

1) No branch resistance and no virtual resistance: In geographically small networks, the interconnect resistances, r_k, are typically small. Theorem below summarizes the results for case with zero branch and virtual resistances.

Theorem 5: Consider N inverters servicing a complex load Z_L (see Fig. 2). Assume there is no branch resistance, no virtual impedance, and suppose the real power consumed by the load is $P_L^* = (E^*)^2/(2R_L)$ when $v_k = E^* \sin \omega_o t$ for all k. We express the summation of commanded power as

$$P_1^* + P_2^* + \ldots + P_N^* = (E^*)^2/(2R_L) + \Delta, \tag{15}$$

where Δ represents the mismatch in actual and commanded power delivery. Furthermore, assume all power generated is consumed by the load. Under such conditions, the steady-state voltage $v_k = v(t)$ for all $k = 1, \ldots, n$ is given by $V_g \sin \omega_o(t)$, where

$$V_g = E^* - (E^* + mR_L)(1 - \sqrt{1 + 4\delta}), \tag{16}$$

with $\delta = (2\Delta R_L)/(E^* + mR_L)^2$, $m = \sum_{i=1}^N \frac{1}{n_i}$. For small δ we obtain $V_g \approx E^* + \frac{4\Delta}{(\frac{E^*}{R_L} + m)}$.

Proof: See the Appendix.

Remark 5: Consider the case where all inverters have the same droop coefficient (i.e. $n_i = n$) and there are N inverters such that $m = N/n$. In this circumstance,

$$V_g \approx E^* + \frac{4n\Delta R_L}{nE^* + NR_L}. \tag{17}$$

Thus, the deviation of V_g from E^* becomes vanishingly small as N increases. This implies that a system with more inverters which delivers power to the same total power

provides tighter voltage regulation in comparison to a system with fewer inverters.

In the case where the total commanded power and actual load power are matched (which implies $\Delta = 0$), we recover $V_g = E^*$.

Corollary 2: Under the conditions in Theorem 5, if n_i and n_j are chosen to satisfy $n_i P_i^* = n_j P_j^*$, then $n_i P_i = n_j P_j$ in steady state.

Proof: From the droop-laws we have $E_i = E^* - n_i(P_i - P_i^*)$ and zero branch resistances implies $E_i = V_g$. It then follows that $n_i(P_i - P_i^*) = n_j(P_j - P_j^*)$. Thus $n_i P_i = n_j P_j$. ■

Remark 6: Note that Theorem 2 suggests a mechanism for power sharing despite mismatched conditions, that is even when $\sum_i P_i \neq \sum_i P_i^*$.

B. Simulation results

The simulation parameters are $R = 0\,\Omega$, $L = 600\,\mu$H, $C = 100\,\mu$F for inverter #1 and $1.2R, 1.2L$, and $1.2C$ for inverter #2. As before, the inner-loop voltage and current compensator transfer functions, $K_{\rm vol}$ and $K_{\rm cur}$, are both assumed to contain poles at $\pm j\omega_{\rm o}$ where $\omega_{\rm o} = 2\pi f_0$ and $f_0 = 60\,$Hz. The two inverters are connected in parallel across a common load. The inner-loop controllers were designed by following a loop-shaping procedure. The sensitivity transfer functions corresponding to $K_{\rm cur}$ and $K_{\rm vol}$, as shown in Fig. 5(a), exhibit bandwidths of approximately 1 kHz and 600 Hz, respectively, and the same controller is used for both inverters. The outer droop control is given by $E_k = E^* - n_k(P_k - P_k^*)$, where $E^* = 120\sqrt{2}\,$V. The value of n_k dictates the deviation of E_k from E^* which in turn also influences reactive power flows according to Corollary 1. Here two scenarios are studied.

1) Symmetric Outer Droop Laws: Figure 5(b) shows that the difference in the inverter currents is negligibly small when the outer-droop laws are the same for the two inverters even when the load has non-unity power factor and the power commanded does not match the active power rating of the load. Since the droop laws are identical for this particular case, both the inverter output voltages deviate by the same amount and thus $\delta_1 - \delta_2 = \frac{E_1 - E_2}{E^*}$ is small. This results in small phase differences between inverter currents (see Corollary 1). Thus, even under a mismatch between active load power rating and total commanded power, $\sum P_k^*$, the phase difference between inverter currents is small. This result also holds for complex loads.

2) Asymmetric Outer Droop Laws: If the load is purely resistive, then the phase difference between inverter currents is zero (see Theorem 3) regardless of mismatches between rated active power of the loads and the total commanded power or mismatched droop slopes among inverters. Simulation results under mismatched droop slopes with a resistive load are presented in Fig. 5(c).

Remark 7: An interesting observation supported both by the analysis and simulations is that if the droop laws are similar then the phase difference in the inverter currents (and therefore the reactive flows) are small. This holds even when the load is complex. In contrast, reactive flow mitigation requires due care under mismatched droop slopes for complex loads. One key insight obtained is that the phase difference between currents can be controlled by ensuring that deviation of all E_k from E^* are similar. Under the conditions of Theorem 5 and from Corollary 2, we can conclude that $E_i - E^* = n_i(P_i^* - P_i) = n_j(P_j^* - P_j) = E_j - E^* = 0$ if we impose $n_i P_i^* = n_j P_j^*$ on design of the droop laws. Evidently in typical scenarios, the conditions of the theorem are not met since branch and virtual impedances are not zero. However branch resistances r_k and virtual resistance $R_{\rm v}$ assume small values and therefore a choice of n_k according to $n_i P_i^* = n_j P_j^*$ can still prove an effective design rule. Fig. 6(a) shows that the inverter current phase differences are small when this guideline is used instead of choosing identical droop coefficients. Also smaller values of $\sum_i n_i P_i^*$ result in smaller phase differences. Higher virtual resistances and branch resistances also result in lower phase differences but at the expense of power sharing accuracy and power loss (see Fig. 6 (b) and (c)). Thus the analysis and simulations indicate the following measures to limit reactive flows: i) choose n_k according to $n_i P_i^* = n_j P_j^*$ (e.g. the reactive phase difference in inverter currents was reduced from -40 deg to -13 deg for a power factor (lagging) of 0.5) ; ii) pick lower $\sum_i n_i P_i^*$; and iii) increase the values of virtual resistance and or the branch resistance to further limit reactive flows. With these design guidelines, reactive power flows can be mitigated.

APPENDIX

Proof of Theorem 1: Note that (9) can be rewritten in terms of *slow* time variable $\tau := \omega_{\rm o} t$ as $\frac{dP_s}{d\tau} =$

$$\epsilon\left(-P_s + \alpha E^2\left(1 - \frac{\cos(2\tau + \phi_i + \phi_v)}{\cos(\angle(Y(j\omega_{\rm o}))}\right)\right) := \epsilon g(P_s, \tau),$$

where $P_s(\tau) = P(t)$. The corresponding averaged equation is given by $\frac{d\bar{P}_s}{d\tau} = \epsilon\bar{g}(\bar{P}_s)$, that is

$$\frac{d\bar{P}_s}{d\tau} = \epsilon\left(-\bar{P}_s + \alpha[E^* - n(\bar{P}_s - P^*)]^2\right),$$

which can be solved to obtain (11).

Let $D = (P(0) - \delta, b + \delta)$ for some $\delta > 0$. Since $\epsilon g(P_s, \tau)$ is in C^1, therefore for L in $(0, \frac{P(0)+b+\delta}{2\sup_{P_s,\tau}\|g(P_s,\tau)\|})$, the solution $P_s(\tau) \in D$ for $0 \leq \tau \leq L/\epsilon$, and we obtain that there exists $c > 0$ such that (using results from averaging theory such as in [12]) $\|P_s(\tau) - \bar{P}_s(\tau)\| < c\epsilon$ for $0 \leq \tau \leq \frac{L}{\epsilon}$. The theorem statement results since $P(t) = P_s(\tau)$. ■

Proof of Theorem 4: We will assume steady state for this proof. Now in the isochronous half-droop method assuming that sinusoids with frequency $\omega_{\rm o}$ are tracked perfectly we can assume that $T(j\omega_{\rm o}) = 1$ and $Q(j\omega_{\rm o}) = -R_{\rm v}$. Also, we assume that $\hat{\boldsymbol{v}}_{\rm ref} = \boldsymbol{E}\mu(s)$ where $\mu(s) = \frac{\omega_{\rm o}}{s^2+\omega_{\rm o}^2}$ is the Laplace transform of a sinusoid with frequency $\omega_{\rm o}$. Thus it follows that $\hat{\boldsymbol{v}} = (I + YR_{\rm v})^{-1}\boldsymbol{E}\mu(s)$, $\hat{\boldsymbol{i}} = Y\hat{\boldsymbol{v}} = Y(I + YR_{\rm v})^{-1}\boldsymbol{E}\mu(s)$, $\hat{v}_L = h(s)\boldsymbol{\lambda}^{\rm T}\hat{\boldsymbol{v}}$, $\hat{i}_L = \frac{\hat{v}_L}{Z_L} = q(s)\boldsymbol{\lambda}^{\rm T}(I + YR_V)^{-1}\boldsymbol{E}\mu(s)$. By using Woodbury matrix inverse identity, we obtain $Y^{-1} =$

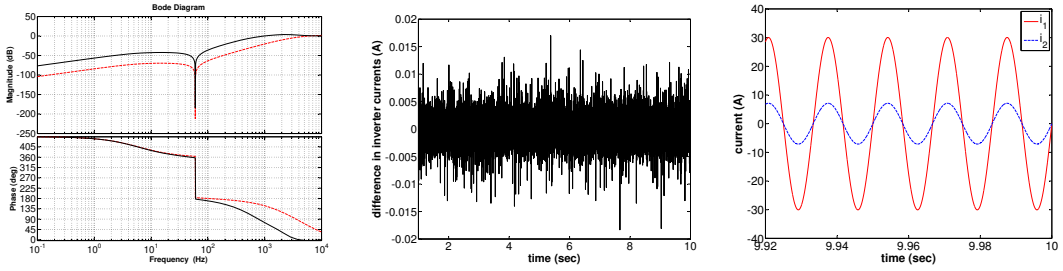

(a) (b) (c)

Fig. 5. (a) Bode plots of the sensitivity transfer functions of the current controller and the voltage controller are shown. Both track 60 Hz sinusoids with negligible error. (b) Difference in inverter currents is negligibly small when the droop law for both inverters is identical even when the total active power commanded is twice the total rated active power of a complex load (load is rated at 3 kW with a power factor of 0.75 and $P_1^* + P_2^* = 6$ kW). (c) Two Inverter currents are in phase when the load is purely resistive (rated at 3 kW). The commanded active power $\sum P_k^*$ is 4.5 kW with $P_1^* = 3.365$ kW and $P_2^* = 1.125$ kW. The droop coefficients are $n_1 = n_2 = n = 0.02$ V/W.

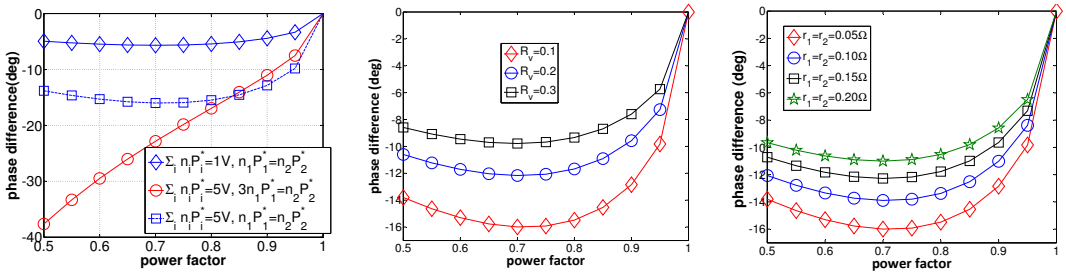

(a) (b) (c)

Fig. 6. (a) Comparison of droop-law designs with different values of $\sum_{i=1}^{2} n_i P_i^*$. Phase differences between inverter currents decrease as the virtual resistances and branch resistances are increased as shown in (b) and (c), respectively. All plots assume asymmetric power sharing $P_1^* = 3P_2^*$ where $P_1^* + P_2^* = 3$ kW. In all scenarios in (b) and (c), $n_i P_i^* = 2.5$V for $i = 1, 2$..

$\mathbf{\Lambda}^{-1} + \eta \mathbf{1}\mathbf{1}^T$, $\eta := \frac{h}{1 - h\boldsymbol{\lambda}^{\mathrm{T}}\mathbf{\Lambda}^{-1}\boldsymbol{\lambda}}$, and $\hat{\boldsymbol{i}} = \mathbf{\Lambda}_v \boldsymbol{E}\mu(s) - \alpha \boldsymbol{\lambda}_v \boldsymbol{\lambda}_v^{\mathrm{T}} \boldsymbol{E}\mu$ where $\boldsymbol{\lambda}_v := (\ \frac{1}{r_1+R_v} \ \ \cdots \ \ \frac{1}{r_N+R_v}\ )^{\mathrm{T}}$, and $\mathbf{\Lambda}_v = diag(\frac{1}{r_1+R_v}, \ldots, \frac{1}{r_N+R_v})$. From $\eta = Z_L$ and $\alpha = \frac{\eta}{1+\eta\boldsymbol{\lambda}_v^{\mathrm{T}}1} = \frac{Z_L}{1+Z_L\boldsymbol{\lambda}_v^{\mathrm{T}}1}$, it follows that in steady state $i_k = (\sum_{i=1}^{m} \frac{E_m}{r_m+R_v}) \frac{1}{r_k+R_v} \gamma_k \sin(\omega_o t + \phi_k)$, where $\gamma_k = \sqrt{(\beta_k - |\alpha(j\omega_o)| \cos\angle\alpha)^2 + |\alpha(j\omega_o)|^2 \sin(\angle\alpha)^2}$, $\beta_k = \frac{E_k}{(\sum_{i=1}^{m} \frac{E_m}{r_m+R_v})}$ and $\tan\phi_k == \frac{\sin\angle\alpha}{\cos\angle\alpha - \frac{\beta_k}{|\alpha(j\omega_o)|}}$.The theorem results on expanding $\tan(\phi_k - \phi_j)$ using the above expression for $\tan\phi_k$, where $1 \le k, j \le N$. ■

Proof of Theorem 5: Note that $\sum_{k=1}^{N} P_k^* = \frac{(E^*)^2}{2R_L} + \Delta$ where Δ represents the mismatch in power. Assuming all the power generated is consumed by the load and that droop-laws are being followed we have:

$$\frac{V_L^2}{2R_L} = \sum_{k=1}^{N} P_k = \frac{(E^*)^2}{2R_L} + \Delta + (E^* - V_L)(\sum_k \frac{1}{n_k}). \quad (18)$$

Define the variable $x := E^* - V_L$. Then

$$\frac{x^2}{2R_L} = \frac{(E^* - V_L)^2}{2R_L} = \frac{1}{2R_L}[V_L^2 + (E^*)^2 - 2V_L E^*]$$

Substituting $\frac{V_L^2}{2R_L}$ from (18) into above equation we have

$$\frac{x^2}{2R_L} - (\frac{E^*}{R_L} + m)x - \Delta = 0.$$

The theorem statement is a direct consequence of solving the above quadratic equation and obtaining the viable solution for V_L. ■

REFERENCES

[1] R.H. Lasseter. Microgrids. In *IEEE Power Eng. Society Winter Meeting*, volume 1, pages 305–308, 2002.

[2] P. Piagi and R.H. Lasseter. Autonomous control of microgrids. In *IEEE Power Eng. Society General Meeting*, volume 1, pages 1–8, June 2006.

[3] M.C. Chandorkar, D.M. Divan, and R. Adapa. Control of parallel connected inverters in standalone ac supply systems. *IEEE Trans. Ind. Appl.*, 29(1):136–143, Jan. 1993.

[4] J. M. Guerrero, J. C. Vasquez, J. Matas, L. G. de Vicuña, and M. Castilla. Hierarchical control of droop-controlled ac and dc microgrids–A general approach toward standardization. *IEEE Trans. Ind. Electron.*, 58(1):158–172, 2011.

[5] Brian Johnson, Ali Davoudi, Patrick Chapman, and Peter Sauer. A unified dynamic characterization framework for microgrid systems. *Electric Power Components and Systems*, 40(1):93–111, Nov. 2011.

[6] N. Pogaku, M. Prodanovic, and T.C. Green. Modeling, analysis and testing of autonomous operation of an inverter-based microgrid. *IEEE Trans. on Power Electron.*, 22(2):613–625, Mar. 2007.

[7] Zhao Wang, Meng Xia, and M. Lemmon. Voltage stability of weak power distribution networks with inverter connected sources. In *American Control Conference*, pages 6577–6582, June 2013.

[8] J. W. Simpson-Porco, F. Dorfler, and F. Bullo. Voltage stabilization in microgrids via quadratic droop control. In *Control and Decision Conference*, pages 7582–7589, Florence, Italy, Dec. 2013.

[9] Qing-Chang Zhong. Robust droop controller for accurate proportional load sharing among inverters operated in parallel. *IEEE Trans. Ind. Electron.*, 60(4):1281–1290, April 2013.

[10] J.M. Guerrero, L. Garcia de Vicuna, J. Matas, M. Castilla, and J. Miret. Output impedance design of parallel-connected UPS inverters with wireless load-sharing control. *IEEE Trans. on Ind. Electron.*, 52(4):1126–1135, Aug. 2005.

[11] A. Yazdani and R. Iravani. *Voltage-Sourced Converters in Power Systems*. Wiley, 2010.

[12] Jan A Sanders, Ferdinand Verhulst, and James A Murdock. *Averaging methods in nonlinear dynamical systems*, volume 59. Springer, 2007.